Meng *et al. Cancer Nanotechnology* (2022) 13:13
https://doi.org/10.1186/s12645-022-00121-2

Cancer Nanotechnology

RESEARCH Open Access

Nanocluster-mediated photothermia improves eradication efficiency and antibiotic sensitivity of *Helicobacter pylori*

Fansen Meng[1], Hongjin Tao[1], Yan Mi[2], Tianyu Yang[2], Xuanping Wang[3], Yuyo Go[3], Yunjuan Lin[1] and Gangshi Wang[1*]

*Correspondence: wanggangshi@hotmail.com

[1] Department of Gastroenterology, The Second Medical Center & National Clinical Research Center for Geriatric Diseases, Chinese PLA General Hospital, Beijing 100853, People's Republic of China
Full list of author information is available at the end of the article

Abstract

Background: *Helicobacter pylori* (*H. pylori*) eradication plays a crucial role in gastric cancer prevention, but the antimicrobial resistance of *H. pylori* is obstructing this elimination process. In this study, we developed nanoclusters (NCs) from $Zn_{0.3}Fe_{2.7}O_4$ nanoparticles using a poly(ethylene glycol)-b-poly(ε-caprolactone)-based nanocarrier as an innovative antibiotic-independent *H. pylori* management.

Results: The nanocluster showed minimal toxicity and maximal biocompatibility. With a low concentration (50 μg/mL) of NCs under a short time period (~ 2 min) of near-infrared (808 nm) irradiation, we kept the culture medium temperature to 41 °C for 20 min with continuous irradiation. The heated NCs exhibited efficient photothermal effects and resulted in an excellent inhibition of *H. pylori* growth, adhesion and ability to induce vacuolization in eukaryotic cells in in vitro investigation. Transmission electron microscopy showed a dramatic morphologic change after NCs photothermia on *H. pylori*, including cell wall and membrane rupture, as well as ribosome damage. Besides, levofloxacin and clarithromycin resistance was decreased after photothermal treatment in *H. pylori* NCTC 11637 and/or clinical strains, however metronidazole resistance was unchanged. We also discovered a significant decrease in the biofilm formation of *H. pylori* under the NCs-based photothermal application, while efflux pump function was unchanged.

Conclusions: Based on this novel NCs-based photothermal approach, we were able to demonstrate in vitro a significant inhibition of both *H. pylori* growth and molecular toxicity, and its improvement in antibiotic sensitivity alone with the eradication of *H. pylori* biofilms previously believed to be tolerant to conventional antibiotics.

Keywords: Photothermal therapy, Zinc ferrite nanoclusters, *Helicobacter pylori*, Biofilm, Antibiotic susceptibility

Background

Helicobacter pylori (*H. pylori*) is one of the most common human pathogens with an infection rate over 50% throughout the world (lerardi et al. 2013; Mane et al. 2010; Uemura et al. 2001). *H. pylori* infection is clearly associated with a wide range of

gastric pathologies, such as chronic gastritis, peptic ulcers, and gastric cancer/mucosa associated lymphoid tissue lymphoma (Kusters et al. 2006; McColl. 2010; Parkin. 2006; Rocha et al. 2015; Uemura et al. 2001). Some studies have stated that *H. pylori* eradication may be the most practical way to reduce occurrence of gastric cancer and peptic ulcer disease and ultimately save lives, showing the importance of reliable eradication methods (Forman and Graham. 2004). The rising rate of antibiotic resistance and the emergence of multidrug-resistant (MDR) *H. pylori* strains during the last decade has reduced the success of eradication therapy, and this can be partially attributed to extended and inappropriate use of antibiotics (Boyanova et al. 2019; Kwon et al. 2003; Peake et al. 2016). The World Health Organization (WHO) has published a list of bacteria that urgently requires new antibiotics to overcome their current antibiotic resistance issues, and *H. pylori* is a high priority on the list (Tacconelli et al. 2018). Extensive research is being carried out on any innovative treatment.

One of these new antibiotics-independent approaches to eradicate *H. pylori* is the usage of nanotechnology. Nanoparticle-based drug delivery systems for targeted treatment of tumor and *H. pylori* have been described (de Souza et al. 2021; Zeng et al. 2017). Among them, light-based treatment has been used to utilize nanomaterials and their composites. Photothermal therapy (PTT) has exhibited great potentials in dealing with drug-resistant bacteria and bacterial biofilms. In recent years, photothermal effect has been reported to possess high light–thermal conversion efficiency under the irradiation of near-infrared (NIR) light (Cheng et al. 2019; Jaque et al. 2014). PTT has several advantages, such as being minimally invasive, remotely controllable and efficient. PTT is regarded as a safe and efficient strategy to manage bacterial infections (Han et al. 2020; Liu et al. 2017). Besides, nanoplatforms with synergistic effects of PTT and chemotherapy in tumor therapy (Li et al. 2021), as well as PTT and light-triggered nitro oxide release in antibacterial and antifungal application (Liu et al. 2021) have been developed to exhibit potential clinical significance. Various mechanisms have been shown to contribute to antimicrobial resistance in *H. pylori*, such as genetic mutations, altered efflux pump activity, and the formation of bacterial biofilms (Cammarota et al. 2012). While the field of *H. pylori* biofilm research is fairly new, groups have already begun to explore alternative therapeutic approaches that may target and eradicate bacterial biofilms including PTT (Gurunathan et al. 2015). PTT was reported to be efficient in treating biofilm-related infections and delayed the development of drug-resistant bacteria (Şen Karaman et al. 2020; Teng et al. 2016; Yu et al. 2019; Yuan et al. 2019). However, the effect of PTT on *H. pylori* biofilms remains to be elucidated.

In this study, we synthetized nanoclusters (NCs) from $Zn_{0.3}Fe_{2.7}O_4$ nanoparticles (NPs) using a PEG-PCL-based nanocarrier, and compared its photothermal effects on *H. pylori* inhibition with NPs. We have also assessed their biological safety, as well as any alteration on antibiotic resistance of *H. pylori* after photothermal therapy. We have also assessed the underlying mechanisms of antimicrobial resistance, including changes in biofilm and efflux pump activity. As the first study of its kind, we have confirmed that the photothermal effect of NCs restrict the growth of *H. pylori* and improve antibiotic sensitivity, providing new ideas and methods for future *H. pylori* treatment.

Material and methods

Materials

H. pylori NCTC 11637, which was kindly provided by the *H. pylori* Strain Pool, Beijing, China, and two *H. pylori* clinical strains (27054 and L2) stored in our laboratory were used in this study. The following chemical materials were bought from Solarbio (China): Cell Count Kit-8, Dulbecco's modified Eagle medium (DMEM), Crystal Violet stain solution (1%), Hoechst 33342, fetal bovine serum (FBS), Prussian blue iron stain kit, phosphate buffered saline (PBS), broth medium, trypsin, and penicillin/streptomycin (10,000 U/mL). Campylobacter agar base was purchased from OXOID.

Synthesis of $Zn_{0.3}Fe_{2.7}O_4$ NPs

$Zn_{0.3}Fe_{2.7}O_4$ NPs were synthesized by the thermal decomposition method (He et al. 2018). First, 2.7 mmol Iron(III) acetylacetonate ($Fe(acac)_3$), 0.3 mmol Zinc(II) acetylacetonate hydrate ($Zn(acac)_2 \cdot nH_2O$), 2 mmol sodium oleate, 4.4 mL oleic acid and 20 mL benzyl ether were added in a four neck flask and mixed by magnetically stirring. The mixture was heated to 120 °C for 30 min with nitrogen flow. Under nitrogen blanketing, the mixture was heated to 295 °C (reflux temperature), and kept refluxing for 2 h. Finally, the mixture was cooled down to room temperature, and was treated by ethanol to precipitated out the NPs.

Nanocluster preparation

Nanoclusters (NCs) loaded with $Zn_{0.3}Fe_{2.7}O_4$ NPs were prepared by the solvent evaporation method. 20 mg $Zn_{0.3}Fe_{2.7}O_4$ NPs and 50 mg m-PEG-PCL were added in 8 mL of tetrahydrofuran (THF) then magnetically stirred for 20 min. Next, the mixture solution was ultrasonicated for 20 min. THF was then removed by rotary evaporation. The prepared aqueous solution was centrifuged at 3000 rpm for 5 min and filtered through a 0.2-μM cellulose acetate filter.

Characterization of NPs and NCs

The morphology of NPs was observed by a transmission electron microscope (Hitachi H-7650). The hydrodynamic particle size was measured using a dynamic light scattering instrument (Malvern ZS90 Red). Optical absorption spectra of the samples were recorded by using a UV–visible spectrophotometer (CARY 300 Conc.) with the wavelength range of 500–900 nm.

Photothermal efficiency

To assess the photothermal efficiency of NPs and/or NCs, a diode laser with a power of 1000 mW and a wavelength of 808 nm was used to irradiate the dispersions of NPs or NCs. Different concentrations of NPs or NCs (0, 25, 50 μg/mL) dispersions diluted in 1 mL PBS in McBurney turbidimetric tubes were exposed to the laser light with a power density of 1.0 W/cm^2. PBS was selected as a control. The temperature rising of dispersions was recorded by thermometer. The temperature rising of dispersions was recorded by thermometer. The thermometer probe was placed vertically in the center of the

samples. The initial distance between laser source and PTAs liquids was 50 cm. When the temperature of the system reached 40.5 °C, the distance was adjusted to around 80 cm to keep the temperature at 41 °C constantly.

Cell culture

BGC-823 cells stored in our laboratory were used and maintained in DMEM//HIGH GLUCOSE medium containing 10% FBS and penicillin/streptomycin (100 μg/mL penicillin and 100 μg/mL streptomycin) and cultured in a humidified atmosphere of 5% CO_2 at 37 °C.

H. pylori culture

H. pylori was cultivated on Campylobacter agar base with 7% sheep blood in a microaerobic condition (5% O2, 10% CO2, 85% N2) at 37 °C. For liquid culture, the medium consisted of Brucella broth contained 10% FBS under agitating conditions (120 r/min) at 37 °C in a microaerobic environment.

Cytotoxicity of $Zn_{0.3}Fe_{2.7}O_4$ NCs on BGC-823 cells

Cell Counting Kit-8 test was used to assess the cytotoxicity of $Zn_{0.3}Fe_{2.7}O_4$ NCs to BGC-823 cells. For the CCK-8 test, the BGC-823 cells were cultured in 96-well plates at a density of 1×10^4 cells per well and were grown 10 h to stick to the wall (n = 5 per group). Then, they were co-incubated with different concentrations (0, 25, 50, 100, 200, 250 μg/mL) of $Zn_{0.3}Fe_{2.7}O_4$ NCs at 37 °C for 24 h and 48 h. After this step, wells were washed th ree times with PBS. Afterward, cells were incubated in media with 10% CCK-8 solution (150 uL) at 37 °C for 1 h in the dark. Following this period, the supernatant (100 uL) was transferred to a new plate to avoid the affect of NCs on optical density (OD) measurement. And finally, the absorbance was measured at 450 nm to quantify the cell growth.

Prussian blue staining

Prussian blue staining was used to assess the cellular uptake of $Zn_{0.3}Fe_{2.7}O_4$ NCs to BGC-823 cells. Different concentrations (25, 50, 100 μg/mL) of $Zn_{0.3}Fe_{2.7}O_4$ NCs were incubated with BGC-823 cells in 24-well plates at a density of 10^5 cells per well (n = 4 per group). After 12 h or 24 h incubation, the cells were washed with PBS for three times, and then fixed with 4% paraformaldehyde. To stain the iron in cell, Prussian blue solution, 2% hydrochloric acid aqueous solution and 2% potassium ferrocyanide (II) trihydrate were mixed, and then incubated with the fixed cells for 30 min at 37 °C. Then, the cells were washed three times, and counterstained with nuclear eosin for 20 s. Finally, the cells were observed by a microscope after washing three times with ultrapure water.

Inductively coupled plasma mass spectrometry (ICP-MS)

$Zn_{0.3}Fe_{2.7}O_4$ NPs or NCs were incubated with BGC-823 cells for 12 h or 24 h in 6-well plates (3×10^5 cells per well). After this, cells were washed five times with PBS, and cells in all wells were collected as one sample (n = 3 per group). Samples were digested with HNO_3 and heated to 80 °C for 3 h for ICP-MS analysis. The Fe content was measured using an Agilent Technologies 7700 × inductively coupled plasma mass spectrometer (Agilent Technologies, Santa Clara, CA).

Effect of $Zn_{0.3}Fe_{2.7}O_4$ NCs heating on *H. pylori* growth

H. pylori in exponential growth phase was collected by PBS.1 ml mixture of NCs (50 μg/mL) and *H. pylori* (1×10^8 CFU/mL) was prepared in a McBurney turbidimetric tube. The tube was heated by with an 808-nm laser and the temperature of the mixture was recorded by a thermometer. 10 μL of the mixture after the heating process was added to 3 mL broth medium and was cultured at 37 °C for 96 h. Then, the absorbance of each group was measured with a spectrophotometer (UV-2000, China) at OD_{600}, which quantified the *H. pylori* survival rate. After heat treatment the mixture was diluted to 4×10^5 CFU/mL and each culturing agar medium was full of 100 μL of the diluted mixture and cultured at 37 °C for 96 h. Finally, each group was counted to quantify the *H. pylori* survival rate.

Transmission electron microscopy

H. pylori in exponential growth phase was collected in PBS, and 1 ml mixture of NCs (50 μg/mL) and *H. pylori* (1×10^8 CFU/mL) were prepared using McBurney turbidimetric tube and the tube was exposed to an 808 nm laser to heat the mixture to 41 °C for 20 min. After centrifugation for 4 min at 1500 r/min, discarding the supernatant. Then, the bacterial was resuspended using a 2.5% glutaraldehyde fixation solution, and the bacteria was fixed at 4 °C. After that, 10 μL of bacterial liquid was dropped on the amorphous carbon-coated copper grids and allowed to dry. Then, one drop of 3% phosphotungstic acid dye solution was added for negative staining. Finally, samples were observed by TEM.

Evaluation of *H. pylori* adhesion ability and vacuolating cytotoxin

H. pylori was collected in PBS and heated to 41 °C for 20 min. The bacteria were dissolved in DMEM/HIGH GLUCOSE medium without antibiotics and serum, to form *H. pylori*–DMEM/HIGH GLUCOSE solution ($OD_{600} = 0.1$) for standby. For adhesion ability, BGC-823 cells were planked in a 96-well plate with 1×10^4 cells/well, and cultured overnight. The above-mentioned bacteria liquid was added for co-cultivation with a ratio of bacteria:cells of 100:1 for 2 h. Then, discarding the supernatant and the cells were washed with PBS three times. Adding 100 μL urea reagent into each well, and incubated for 2 h at room temperature. Finally, the absorbance of each group was measured with a spectrophotometer at a wavelength of 540 nm. For vacuolating cytotoxin, BGC-823 cells were planked in 96-well plate with 5×10^3 cells per well, and incubated at 37 °C overnight. The above-mentioned bacteria liquid was added for co-cultivation for 24 h with a ratio of bacteria:cells of 200:1.The supernatant was discarded and 100 μL neutral red (0.005%) was added into each well for 5 min. Then, discarding the dye, and washing the cells with PBS three times, and 100 μL hydrochloric acid alcohol (0.04%) was added into each well. The absorbance of each group was measured with a spectrophotometer at a wavelength of 550 nm.

Assessment of *H. pylori* susceptibility to antibiotics

MIC of various antibiotics for NCTC 11637 and all the clinical strains were measured by the Epsilometer test (E-test) using an E-strip (Liofilchem, USA). All the strains

cultured in agar medium, and the third-generation colonies were selected and suspended in PBS to an OD_{600} of 1 for standby. For control groups, above-mentioned bacteria solution were diluted to $OD_{600} = 0.1$ and 100 μL of the bacterial solution was coated on Karmali agar base evenly. After each agar plate was left to dry, E-strip was affixed, and then the plates were incubated at 37 °C under microaerobic conditions, and MIC values were determined after 72 h. The method used to determine the MICs for heated groups was similar to that used for the control groups, 100 μL of the bacterial solution ($OD_{600} = 1$) was exposed to an 808 nm laser to heat to 41 °C for 20 min, then was evenly coated on Karmali agar base to determine the MIC values.

Crystal violet staining

Biofilm formation was assessed under agitating conditions (120 r/min) in 12-well plates. *H. pylori* was collected by PBS and resuspended to an OD_{600} of 1, and further diluted to 5×10^5 CFU/mL in broth medium and each was filled with 3 mL of the diluted bacterial solution and incubated at 37 °C for 4 days. The plates were washed with PBS three times gently, and then stained with 500 μL of 1% (w/v) crystal violet for 30 min. The crystal violet stain was solubilized with 80% ethanol–20% acetone solution, and then measuring the absorbance at OD_{580}. For experimental groups, the samples were heated with NIR to 41 °C last for 20 min, and the remaining steps were the same as above after a generation of cultivation.

Confocal laser scanning microscopy (CLSM)

CLSM was aimed at observing the biofilm as described with slight modifications (Takenaka et al. 2001). A biofilm model of *H. pylori* was constructed in 6-well cell culture plate. Sterile cover glass with a diameter of 1 cm was put into 6-well plates, and 3 mL broth medium was added into each well. Then 10 μL *H. pylori* solution with an OD_{600} of 1 was added into each well. The bacteria were cultured for 4 days in an incubator at 37 °C. The cover glass was removed, washed 3 times in PBS buffer to remove excess planktonic bacteria, and then moved into a new 6-well plate and fixed in 2.5% glutaraldehyde at 4 °C for 1.5 h. After washed with PBS, the fixed cover was added 300 μL FITC-ConA (100 mg/mL) for 30 min at 4 °C away from light, and PBS buffer was used to rinse slowly twice. Then, equal PI staining was performed in the same way and the cover glass was dried at room temperature away from light. Afterwards, the cover glass was sealed with anti-fade mounting medium, then observed under a laser confocal microscope. Five fields of the slides were randomly selected for shooting.

Hoechst 33342 accumulation assay

Accumulation assay was performed as described previously (Coldham et al. 2010). *H. pylori* was collected by PBS and resuspended to an OD_{600} of 1, Then, 180 μL of this bacteria solution was added to 96-well plate. The excitation and emission wavelengths were 355 and 460 nm, respectively, using SpectraMax M5/M5e (USA). After adding Hoechst 33,342 (25 μM, 20 μL) 5 min, recordings were started. Readings were taken every 75 s for 30 cycles, and each experiment was repeated three times. For experimental groups, the samples were heated with NIR to 41 °C for 20 min, and the remaining steps were the same as above after a generation of cultivation.

Statistical analyses

Statistical analysis was carried out using GraphPad Prism (GraphPad Software, Inc., San Diego, CA, USA). All data were present as mean ± standard errors of the means and determined using Student's t-test. For all analyses, p values < 0.05 were considered significant, and the level of significance was described as *p < 0.05, **p < 0.01, ***p < 0.001.

Results

Synthesis and characterization of nanoclusters

The NPs were synthesized by the one-pot thermal decomposition method, and the nanoclusters were prepared by a solvent evaporation method (Additional file 1: Fig. S1). Figure 1a is the transmission electron microscopy (TEM) of $Zn_{0.3}Fe_{2.7}O_4$ NPs deposited on an amorphous carbon-coated Cu grid. The average diameter of monodisperse $Zn_{0.3}Fe_{2.7}O_4$ NPs was about 18 nm with a tight size distribution. The result of electron diffraction pattern shows that $Zn_{0.3}Fe_{2.7}O_4$NPs have high degree of crystallinity with typical cubic spinel structure (Fig. 1b). Figure 1c is the TEM image of $Zn_{0.3}Fe_{2.7}O_4$ NCs formed by PEG-PCL nanocarriers. The size distribution of nanocluster in aqueous solution was measured by dynamic light scattering, as shown in Fig. 1d. The nanoclusters have a hydrodynamic size of about 130 nm with a relative broad size distribution. Figure 1e shows the optical absorption spectra of $Zn_{0.3}Fe_{2.7}O_4$ NPs dispersion. The absorption curve exhibits a platform with relative high value at the wavelength from 750 to 850 nm, indicating $Zn_{0.3}Fe_{2.7}O_4$ nanoclusters with good photothermal performance in the first NIR biological window.

NPs or NCs in phosphate buffered saline (PBS) solution were exposed to 808 nm lasers to study the photothermal efficiency. The time required for the solution to rise to 41 °C

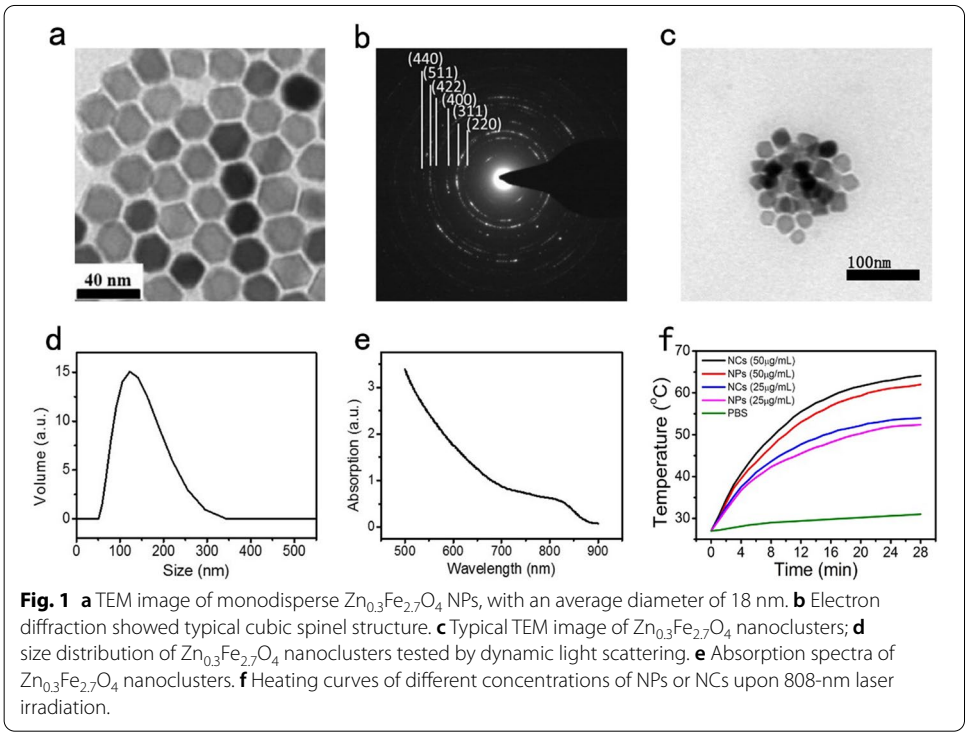

Fig. 1 **a** TEM image of monodisperse $Zn_{0.3}Fe_{2.7}O_4$ NPs, with an average diameter of 18 nm. **b** Electron diffraction showed typical cubic spinel structure. **c** Typical TEM image of $Zn_{0.3}Fe_{2.7}O_4$ nanoclusters; **d** size distribution of $Zn_{0.3}Fe_{2.7}O_4$ nanoclusters tested by dynamic light scattering. **e** Absorption spectra of $Zn_{0.3}Fe_{2.7}O_4$ nanoclusters. **f** Heating curves of different concentrations of NPs or NCs upon 808-nm laser irradiation.

of NCs (50 μg/mL) and NPs (50 μg/mL) was 240 s and 300 s, respectively. It took longer at lower concentrations (25 μg/mL) to reach to 41 °C, and PBS alone has no appreciable temperature rise (Fig. 1f). These results indicate that the photothermal converting efficiency of NPs or NCs dispersed in PBS solution is dose-dependent.

Biosafety evaluation of NCs and its heating effects on *H. pylori* growth

Cell Counting Kit-8 (CCK-8) assay indicated that when human gastric adenocarcinoma epithelial cells BGC-823 cells were cultured with various concentrations of NCs (range: 0–250 μg/mL) for 24 h or 48 h, cell viability was not affected until the concentration reached 200 μg/mL. When the concentration reached 250 μg/mL, an inhibitory effect on cell viability was observed (Fig. 2a). After co-culturing with NCs (300 μg/mL) for 48 h, the BGC-823 cell counts decreased to 50% of that in the control group (Additional file 1: Fig. S2).

Mammalian cell uptake and penetration of NCs and NPs were investigated: BGC-823 cells were cultured with different concentrations of NPs and NCs (0, 25, 50, 100 μg/mL) for 12 h and 24 h. In the NPs group, the cytoplasm was stained blue (indicating endocytosis) at 50 μg/mL at 12 h, and at 25 μg/ml at 24 h. The NCs group showed no cytoplasm staining at 100 μg/mL at 24 h. The results demonstrated that, compared with NPs, NCs showed no internalization into gastric cancer cells even at a high concentration and long incubation time (Fig. 2b), which illustrated the biosafety aspect of NCs as a photothermal hyperthermia agent. In addition to this experiment, we have incubated Prussian blue with NPs and NCs for 12 h, after the washing process, both samples still demonstrated blue color compared to the control group. This result proved that Prussian blue could penetrate PEG membrane and enter inside NCs, therefore when NCs infiltrated into cells they could be identified by dyed blue stainings (Additional file 1: Fig. S3).

We further quantified the NCs and NPs cellular uptakes in BGC-823 cells by measuring iron (Fe) content, through inductively coupled plasma mass spectrometry (ICP-MS). After 24 h, no significant difference in Fe content was observed between control group and NCs co-cultured group. In contrast, the ICP-MS showed a significant increase in the uptake of NPs in BGC-823 cells after 24 h of incubation, and Fe concentration was time-dependent (Additional file 1: Fig. S4).

We then investigated the photothermal effects of NCs on *H. pylori* growth and bacteria toxicity. A NIR laser at 808 nm was applied to NPs and NCs to heat the solution. The real-time monitoring of temperature in the culture solution during the laser irradiation was performed using a thermometer placed in the solution. Bacterial colony counts and OD_{600} values measured by a spectrophotometer were used for representing the growth of bacteria. The growth inhibition rate of *H. pylori* after NCs photothermia increased monotonically in a temperature-dependent and time-dependent way, as shown in Additional file 1: Fig. S5. Based on the photothermal efficiency and cell uptake test results, we chose a concentration of 50 μg/mL NPs or NCs in the planktonic *H. pylori* cultures which were then applied with laser irritation to increase the temperature to 41 °C for 20 min. NCs heat treatment group showed a significant inhibition to growth of *H. pylori*, with the cell growth of 6.7% that of the control group ($n = 3$, $p < 0.001$) (Fig. 3a). NCs without NIR irradiation group and the 41 °C water bath group had no influence on bacterial growth (Fig. 3a). The inhibitory efficiency of NCs group was superior to the NPs

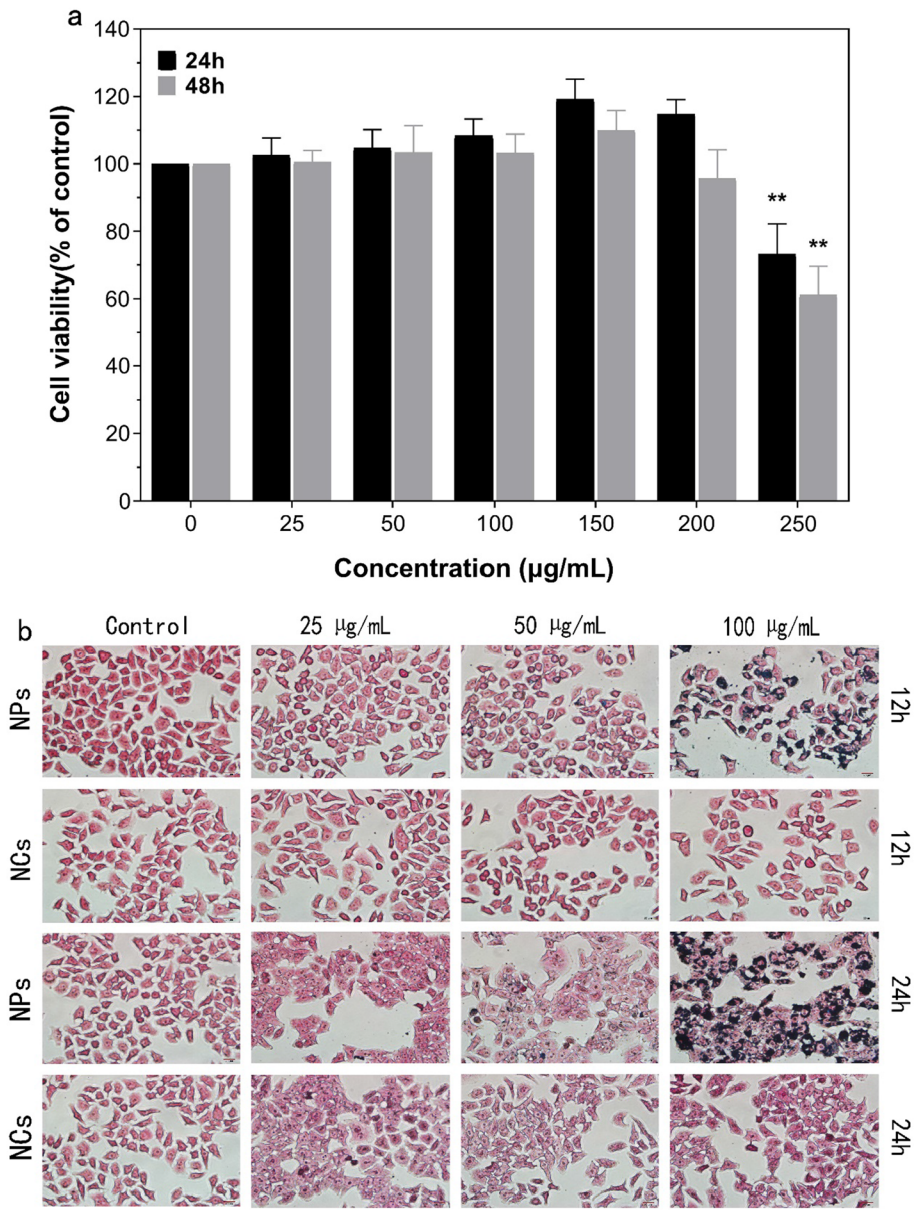

Fig. 2 **a** The cytotoxicity of NCs to BGC-823 cells determined by CCK-8 assay. Cell viability was represented by optical density (OD) values measured by a spectrophotometer at a wavelength of 450 nm. ** $p < 0.01$, compared with 0 μg/ml group (control group); **b** BGC-823 cells were incubated with NPs and NCs in the concentration range from 0 to 100 μg/mL for 12 h and 24 h, respectively. The cells were stained blue in the NPs group at the concentration of 50 μg/mL at 12 h, and 25 μg/mL at 24 h. The NCs group showed no cytoplasm staining at the concentration tested (400 ×).

groups (Additional file 1: Fig. S6). Two clinical *H. pylori* stains (No. 27054 and No. L2) treated by laser irradiated NCs heating also demonstrated similar results (Fig. 3b and c). It is also notable that *H. pylori* growth inhibition after NCs heating was both concentration-dependent and time-dependent: the 50 μg/mL group showed a better inhibitory effect than the 25 μg/mL group, and the inhibitory effect in 20 min group was higher than in the 10 min group (Fig. 3d–f).

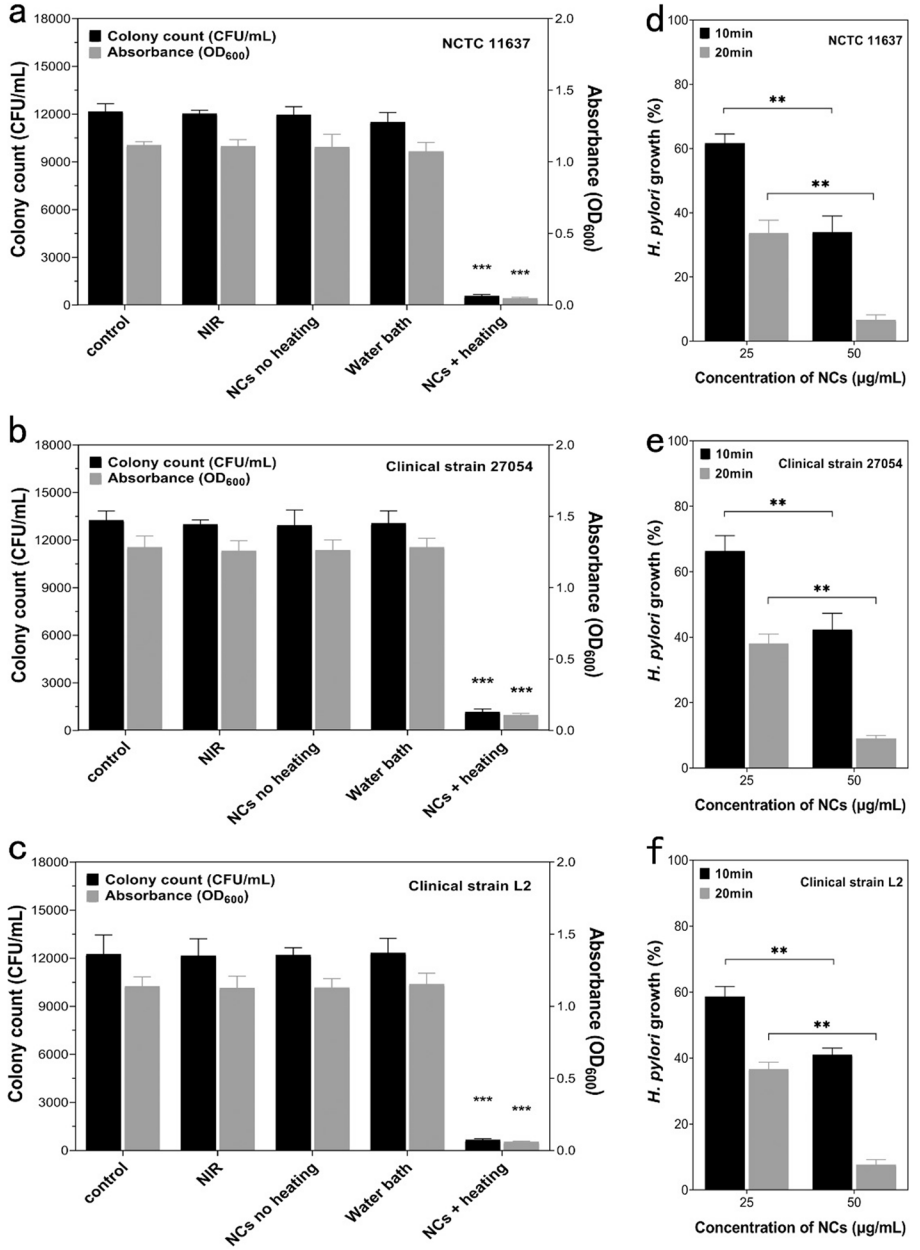

Fig. 3 Effects of $Zn_{0.3}Fe_{2.7}O_4$ NCs photothermia on the growth of *H. pylori*. Left panel: growth of **a** NCTC 11637, **b** clinical strain 27054, **c** clinical strain L2, after different treatment. *H. pylori* amount was measured by both colony count (CFU/ml) and absorbance of OD_{600}. NCs plus heating group demonstrated significant inhibition effect on *H. pylori* growth in all strains, *** $p < 0.001$, compared with control. In contrast, interventions such as NIR, NCs without NIR irradiation, water bath at 41 °C, showed no growth inhibition. Right panel: growth of **d** NCTC 11637, **e** clinical strain 27054, **f** clinical strain L2 after different heating time and concentration of NCs. In equal heating time, NCs in higher concentration illustrated better *H. pylori* inhibition effects. When the NCs concentrations were equivalent, more heating time equaled better effects. The group of 50 ug/mL NCs photothermia at 41 °C for 20 min exhibited the best efficiency (n = 3), ** $p < 0.01$

While *H. pylori* cells growth was inhibited, the bacterium itself experienced several changes limiting its toxicity. In *H. pylori* 11637, the NCs photothermia group showed significantly lower adhesion ability of *H. pylori* cells compared with the control group

(n = 3, $p < 0.001$). NC photothermia groups also exhibited less cell vacuolization, with a 29.2% reduction compared with the control group (n = 3, $p < 0.001$) (Additional file 1: Fig. S7).

Effect of NCs photothermia on the morphology of *H. pylori*

The effects on the morphology of *H. pylori* by NCs photothermia can be visualized through TEM. In the control sample, typical appearances of the *H. pylori* bacteria can be seen, with most having intact outer and inner membrane, complete ribosomes, and uniform cytoplasm (Fig. 4, control). In the NCs photothermia sample, the addition of heat resulted in a partial disappearance and thinning and shrinking of the outer membranes, abnormal distribution or disappearance of internal structures such as ribosome, and leakage of cytoplasmic contents (Fig. 4, NCs + heating).

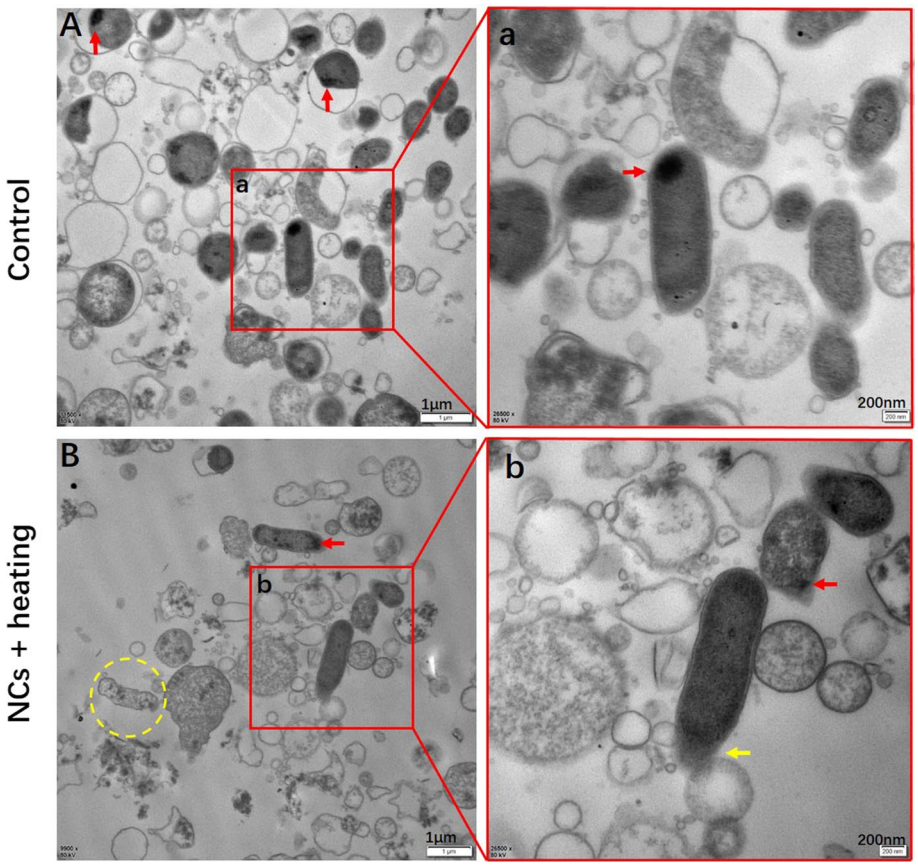

Fig. 4 Effects of NCs heating on *H. pylori* morphology under transmission electron microscopy observation. Upper lanes: control group, *H. pylori* appeared in orderly distribution with intact cell wall and membrane. The cytoplasms were uniform with medium electron density. Ribosomes were intact as indicated by red arrows in A and a; lower lanes: NCs heating group, *H. pylori* were dispersed and disorganized. Yellow circle in B demonstrated distorted bacteria with thin and incomplete cell wall. Abnormal ribosome (red arrows in B and b) and leakage of cytoplasmic contents (yellow arrow in b) were observed. The red squares (a and b) demonstrated higher magnification of A and B, highlighted cell wall and membrane changes of individual *H. pylori*

Induced changes in antimicrobial susceptibility of *H. pylori*

We tested NPs and NCs heating on *H. pylori* strains using the E-test strip, in order to test its susceptibility to antibiotics (levofloxacin, clarithromycin and metronidazole). The minimum inhibitory concentration (MIC) for levofloxacin of 11637 was 1.4 μg/mL (control group). After photothermal heating at 41 °C for 20 min, MIC of *H. pylori* to levofloxacin decreased to 0.3 μg/mL in the NPs group and 0.8 μg/mL in the NCs group, which were below the breakpoint of levofloxacin resistance (1.0 μg/mL) (European-Committee. 2021). Two levofloxacin-resistant clinical strains were also tested (27054 and L2), they were no longer resistant to levofloxacin after photothermia process. The MIC for clarithromycin of a clarithromycin-resistant clinical stain (27054) decreased after photothermia, but the value was still above the breakpoint of resistance. *H. pylori* NCTC 11637 strain and clinical strain (L2) were sensitive to clarithromycin before the heating, and this did not change after photothermia (Table 1, Additional file 1: Fig. S8). All of these clinical strains remained metronidazole-resistant before and after heating.

Biofilm and efflux pump function test of *H. pylori* after NCs photothermia

We therefore investigated whether biofilms alteration played a role in the decrease of *H. pylori* antimicrobial sensitivity in our NC experiments.

Crystal violet staining (Fig. 5a and b) and confocal laser scanning microscopy (CLSM) (Fig. 5c) were used to observe the changes of biofilms produced by NIR heating. Figure 5a shows that biofilms were produced at the air–liquid interface on 12-well plates after 4 days of shaking culture in broth medium supplemented with 7% fetal bovine serum (FBS). Compared with the control group, the bacteria heated by NCs-based NIR produced less biofilms, and the two clinical strains were consistent with NCTC 11637. Biofilms were quantified using a spectrophotometry-based approach, as in Fig. 5b, and the ratio of biofilm to biomass was significantly reduced in *H. pylori* treated with NIR heating. We also compared the control group with the treatment group by CLSM (Fig. 5c). We added fluorescein isothioyanate concanavalin A (FITC-ConA) and propidium iodide (PI) to both groups, and FITC-ConA would show green fluorescence where biofilm were formed, while PI would display red fluorescence when *H. pylori* was

Table 1 Summary of antibiotic susceptibility of *H. pylori* strains under different conditions

***H. pylori* strain**	**Antibiotics**	**MIC (μg/mL)**		
		Control	**NPs (41 ℃ 20 min)**	**NCs (41 ℃ 20 min)**
11,637	Levofloxacin	1.4	0.3	0.8
	Clarithromycin	0.125–0.25	0.125–0.25	0.125–0.25
	Metronidazole	> 256	> 256	> 256
27,054	Levofloxacin	1.1	0.8	0.5
	Clarithromycin	16–24	8–12	6–8
	Metronidazole	> 256	> 256	> 256
L2	Levofloxacin	1.2	0.7	0.5
	Clarithromycin	0.125–0.25	0.125–0.25	0.125–0.25
	Metronidazole	> 256	> 256	64–96

MIC breakpoints (μg/mL) (European-Committee): levofloxacin: sensitive (S) ≦ 1, resistant (R) > 1; clarithromycin: S ≦ 0.25, R > 0.5; metronidazole: S ≦ 8, R > 8

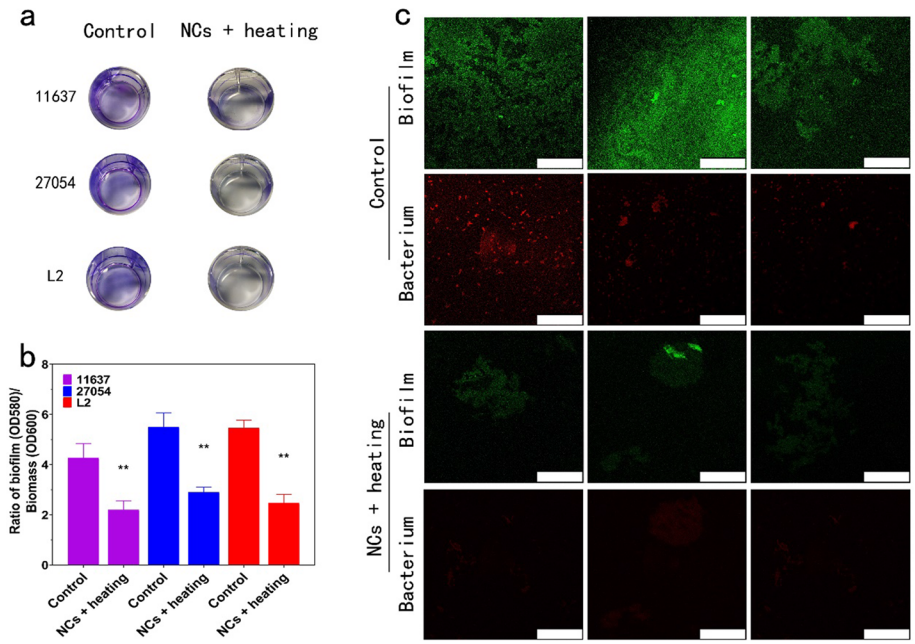

Fig. 5 Effects of photothermia on *H. pylori* biofilm formation. **a** Macroscopic observation assessed by crystal violet staining in 24-well plate after 4 days of culture. Compared with control, no obvious violet signal was observed in the NCs + heating group, including *H. pylori* NCTC 11637 as well as two clinical strains (27054 and L2). **b** Changes of biofilm-to-biomass ratios of *H. pylori* NCTC 11637, clinical strain 27054 and L2. Bar graph represents mean biofilm-to-biomass ratios ($A_{580}/A_{600} \pm$ standard error of the mean). ** $p < 0.01$, vs. the control group, n = 3. **c** Confocal laser scanning microscopy (CLSM) images of *H. pylori* NCTC 11637 strain biofilms. Cells stained with FITC-ConA (green) which represented the biofilm and PI (red) which represented *H. pylori* were visualized by confocal microscopy (400 ×), scale bars 25 μm

detected. As can be seen in Fig. 5c, the control group has showed strong green fluorescence and formed large mature biofilms with compact structures. In the treatment group, the green fluorescence was weaker and the biofilms were discontinuous with larger apertures than the control group. Therefore, CLSM also indicated the photothermal effect of NCs exerted on *H. pylori* biofilms, and this might be a significant factor in the change of drug sensitivity of *H. pylori* in the experimental group.

In addition, we explored whether the photothermal effect of NCs could affect the efflux pumps of *H. pylori*. As shown in Fig. 6, we did not find any difference in accumulation of Hoechst 33342 between the experimental (NCs + heating) group and the control group, indicating that the photothermal effect of NCs has no effect on the function of efflux pumps, in contrast to the high fluorescence in CCCP group caused by suppressed efflux pump function.

Discussion

As the essential elements in PTT, photothermal agents can transform light energy into heat to cause membrane rupture, protein denaturation and irreversible bacterial destruction (Li et al. 2019). Metallic compound nanocomposites (metal sulfide/oxide) have been investigated as bactericidal agents, due to their source variety, high stability, semiconductor characteristics, good biocompatibility, easy preparation,

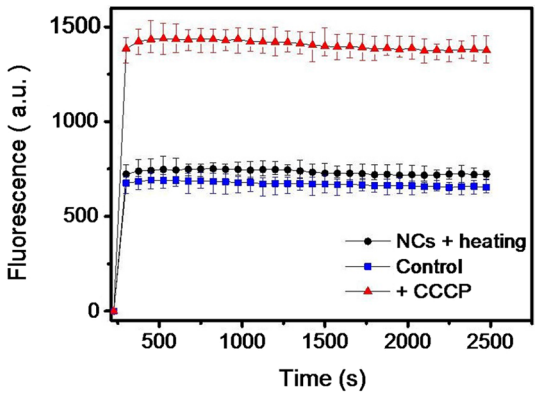

Fig. 6 Comparison of the accumulation of Hoechst 33342 (2.5 μM) in biofilm cells of the control, treated strains. Effect of efflux pump inhibitors CCCP (10 μM) on the accumulation of Hoechst 33342 (2.5 μM) by control, treated strains was used as positive control. The fluorescence intensity was recorded at excitation and emission wavelengths of 350 nm and 460 nm, respectively, over a 30-min incubation period. The data presented are the means ± standard errors of the means from three separate experiments

low cost, and photothermal conversion efficiency. It is reported that low concentrations (10 mg/mL) of $ZnFe_2O_4$–rGO nanostructures under NIR irradiation for a short time period (~ 1 min) exhibited efficient photothermal effects and resulted in effective destruction of cancer cells in in vitro investigation (Akhavan et al. 2014). This highlights the high thermal conversion efficiency of zinc–iron oxide nanostructures, reports have also stated its excellent magnetic thermal conversion efficiency compared to ordinary Fe_3O_4 (He et al. 2018). In this study, the photothermal effect of NCs tended to be more effective and efficient than that of NPs of $Zn_{0.3}Fe_{2.7}O_4$. Zinc oxide nanoparticles have been researched for clinical applications, it demonstrated antiproliferation efficacy in A549 (human lung adenocarcinoma) cells, and with hyperthermia, they revealed cytotoxicity against breast cancer cells and bone cancer cells (Kim et al. 2018; Vimala et al. 2017). In addition, in vivo study to evaluate the efficacy of zinc oxide nanoparticles as an anti-tumor agent demonstrated that rats with hepatocellular cancer treated with zinc oxide had a significant reduction in serum tumor markers such as alpha-fetoprotein, relative to the control group (Hassan et al. 2017). The physiological gastric environment may be hostile to NCs due to its acidic nature, however, with the prescription of proton pump inhibitors (PPI) the environment can be adjusted to a neutral pH value (6–7) (Freedberg et al. 2014). These results indicate the promising possibilities of photothermal therapy in clinical application. By clustering the nanoparticles, we believe that there will be an increased absorption of the indicated radiation, leading to a more efficient conversion of energy into heat than individual nanoparticles. Our results in this study demonstrated that $Zn_{0.3}Fe_{2.7}O_4$ NCs exhibited better photothermal performance than NPs did. Similar biocompatible nanoclusters were developed, with CoMn–iron oxide nanoparticles clustered inside a poly(ethylene glycol)-b-poly(ε-caprolactone) (PEG-PCL)-based nanocarrier. The nanoclusters were found to be safe and exhibited high heating efficiency, which can elevate the intratumoral temperature to 44 °C in the presence of a safe alternating magnetic field (Albarqi et al. 2019).

Reliable biosafety in the human body is essential for any treatment. Good PTAs should have minimal toxicity and maximal biocompatibility. Iron oxide nanoparticles (IONs) stand out as suitable for PTT because of their biocompatibility, biodegradability, simple synthesis, and the ease with which they may be adapted and functionalized for specific applications (Revia and Zhang. 2016). Despite the potential of PTT in antibacterial use, its non-specific heat damage to nearby tissues is potentially concerning. Unlike intracellular hyperthermia of tumors when internalization of nanoparticles into cells is crucial, it is important to avoid adjacent tissue damage during antibacterial applications. This will require prevention of individual nanoparticles being endocytosed by gastrointestinal mucosa cells. In this study, we evaluated biosafety by its invasion on mammalian cell viability and penetration. In order to minimize non-specific heating of healthy tissues, we proposed a controlled clustering of nanoparticles, which will increase the hydrodynamic size of the particles and in turn reduce the chance of internalization into adjacent cells. As studies have successfully demonstrated nanoparticles up to 5–10 μm entering human tissue, there does not seem to be an absolute limit in size that prevents internalization (Gratton et al. 2008). That being said, a smaller nanoparticle is generally considered to have a faster internalization than larger particles with the same charge and clinical composition, one study stated that nanoparticle will encounter difficulty entering cells when the size is greater than 60 nm, due to cellular receptor shortage and entropic penalty (Debbage and Jaschke. 2008; Hoshyar et al. 2016; Sahay et al. 2010). Focusing specifically on gastric cells, smaller polysterene nanoparticles (44 nm) showed a faster and higher proportion of internalization than larger polysterene nanoparticles (100 nm) (Forte et al. 2016). Therefore, by clustering the nanoparticles, we theorized a reduced internalization into adjacent tissues, thus leading to a lower risk of non-specific heating. The ICP-MS results confirmed that NCs could not penetrate into cells easily and demonstrated good biosafety, and this was consistent with our Prussian blue staining findings. These findings could be explained by the size of NCs (ours is 130.1 ± 5.2 nm) which made it difficult to penetrate mammalian cell membrane.

Declining eradication rates of *H. pylori* worldwide related to antimicrobial resistance have inspired a switch from antibiotic-based regimens to novel therapeutic strategies such as nanoparticle-based approaches. In recent years, nanomaterials have exhibited great potential in the growth inhibition of *H. pylori* (Yang et al. 2020; Zhang et al. 2020). Besides, the photothermal anti-*H. pylori* effect of nanomaterials was evaluated effectively in vitro and in vivo (Zhi et al. 2019). In this study, *H. pylori* growth was significantly inhibited after NCs photothermia, while TEM visualized outer wall rupture and ribosomal damage of *H. pylori* cells, which can be indicative of the antibacterial effects of this therapy. *H. pylori* adhesion ability is particularly crucial for its virulence, since adhesion molecules on its surface are responsible for mucin binding, leading to gastric mucosa invasion (Huang et al. 2016). Vacuolization is also significant in *H. pylori*'s toxicity, vacuolating cytotoxin (VacA) itself is a major virulence factor (Palframan et al. 2012). In our study, the NCs photothermia groups showed significantly lower adhesion ability of *H. pylori* cells and reduced cell vacuolization compared with the blank control group. This shows nanoparticle photothermia could be an efficient method to combat *H. pylori* for potential clinical use, both on its growth restriction and on molecular toxicity inhibition.

Alteration of antimicrobial susceptibility was reported after hyperthermia on *Staphylococcus aureus*, *Escherichia coli*, *Pseudomonas aeruginosa*, and our previous study found that NPs magnetic local heating could not only disrupt *H. pylori* cell directly, but could also enhance its susceptibility to amoxicillin, of which could be adopted for clinic applications readily (Alumutairi et al. 2020; Fang et al. 2017; Ma et al. 2019; Nguyen et al. 2016; Wu et al. 2019). One crucial mechanism of drug resistance is the formation of biofilms. Biofilms can be described as adherent aggregates of microorganisms encased in an extracellular polymeric substance (EPS), which contains proteomannans, LPS-related structures, extracellular DNA, proteins, and outer membrane vesicles (Flemming et al. 2016; Hathroubi et al. 2018). In addition, biofilms are associated with increasing mutations (to interfere with the antimicrobial activities), quorum-sensing-regulated mechanisms and the activation of the general stress response. This activity makes it difficult to achieve effective antibiotic activity (Høiby et al. 2010). *H. pylori* is a biofilm-producing bacteria: it forms biofilms on the surface of the gastric mucosa (adopting the biofilm mode of growth to the mucosa and glands and can cover up to 97.3% of cell surface) and it displays resistance to antibiotics including clarithromycin (Hathroubi et al. 2018). Specifically, the MIC increased 16-fold and the minimum bactericidal concentration increased by up to fourfold in biofilm cells compared to planktonic ones (Alumutairi et al. 2020). In general, relatively little is known in the field of *H. pylori's* biofilm structure and genes, and the therapies aiming to dissolve biofilms are still in their infancy (Yonezawa et al. 2015). Our findings provide a novel way to target *H. pylori* antibiotic resistance by the inhibition of biofilm formation.

Carbonyl cyanide m-chlorophenylhydrazone (CCCP), as a transmembrane proton gradient-collapsing agent, is a frequently used proton-transporting ionophore that transmits protons to disrupt transmembrane electrochemical gradient and inhibits the efflux pumps driven by hydrogen ion gradients, and thus restoring the antibiotic sensitivity of bacteria, including *H. pylori* (Fanelus and Desrosiers. 2013; Zhang et al. 2010). Hoechst 33342, a fluorescent probe, is a substrate for a wide range of bacterial multidrug resistance transporters (Coldham et al. 2010; van den Berg van Saparoea et al. 2005), it can penetrate into *H. pylori* and can be extruded by efflux pump, thus its fluorescence represents not only the amount of Hoechst 33342 in the bacteria, but also the efficiency of efflux pump too. The involvement of efflux pump in multidrug resistance of *H. pylori* has been identified (Bina et al. 2000; Cai et al. 2020; Liu et al. 2008; van Amsterdam et al. 2005). There is no evidence in this study that the function of efflux pumps was affected by NCs photothermia, however, the thinning of the outer membrane may be indicative of the mechanism behind increased antimicrobial sensitivity and the growth inhibition of *H. pylori*.

There was potential limitation to this measurement: although the temperature of the mixture was kept at 41 °C, the interior of NCs and NPs were likely to be much hotter than the macroscopic solution. Studies showed that the temperature around nanoparticles could be detected by using real-time molecular temperature probes and found to decrease exponentially with the increase of distance from the surface of nanoparticles (Riedinger et al. 2013). Acute temperature monitoring of the immediate nanoenvironment around nanoparticles may help to optimize local temperature controls for physical and biomedical applications. As the cooperative effects of antibiotics and NCs heating

may reduce the dose of antibiotics required in the eradication of *H. pylori* greatly, it will be of great interest to couple antibiotics with NCs which can be localized to gastric area and then optimize the synergistic effects. Besides, for the envision that this approach can be applied to clinic applications, in vivo studies are needed to investigate both the anti-*H. pylori* effects of NCs photothermia and its biosafety.

Conclusions

In this study, we successfully designed NCs formed by PEG-PCL-based NPs and demonstrated antibacterial effect of NCs/NPs under NIR laser heating for the first time. We evaluated the biosafety of NCs and NPs, finding that NCs have higher biosafety compared with NPs. We found that NCs could inhibit the growth of *H. pylori* significantly under NIR laser heating. In addition, after NCs local heating, we found MIC of *H. pylori* to levofloxacin and clarithromycin to be decreased. Investigating further, we demonstrated for the first time that the photothermal effect of NCs disrupted *H. pylori* biofilm formation in vitro. Considering the current data, our research provides a new method for treating *H. pylori* infection, especially for drug-resistant strains.

Abbreviations

CCCP: Carbonyl cyanide m-chlorophenylhydrazone; CLSM: Confocal laser scanning microscopy; DMEM: Dulbecco's modified Eagle medium; EPS: Extracellular polymeric substance; E-test: Epsilometer test; FBS: Fetal bovine serum; FITC-ConA: Fluorescein isothiocyanate concanavalin A; *H. pylori*: *Helicobacter pylori*; ICP-MS: Inductively coupled plasma mass spectrometry; IONs: Iron oxide nanoparticles; NCs: Nanoclusters; NIR: Near-infrared; NPs: Nanoparticles; PCL: Poly(ε-caprolactone); PI: Propidium iodide; PTAs: Photothermal agents; PTT: Photothermal therapy; TEM: Transmission electron microscopy; Min: Minute; H: Hour; S: Second.

Supplementary Information

The online version contains supplementary material available at https://doi.org/10.1186/s12645-022-00121-2.

Additional file 1: Fig. S1. The schematic illustration of synthesis of Zn0.3Fe2.7O4 NCs. **Fig. S2**. Effects of NCs on BGC-823 cells growth. NCs were added into the culture medium and cells were observed by inverted microscope (40×) after co-culturing for 48 h. (A) Control group; (B) NCs (300 μg/mL) group exhibited significant growth inhibition of BGC-823 cells. **Fig. S3**. Prussian blue staining of NPs and NCs. NPs and NCs were incubated with Prussian blue for 12h, then washed and observed. NPs/NCs in the control group (no incubation) showed brownish grey. After incubation with Prussian blue, both NPs and NCs were stained blue (400×). **Fig. S4**. Cellular uptake of NPs/NCs in co-cultured BGC-823 cells as quantitatively determined by ICP-MS.*** $p < 0.001$, vs. the control group, $n = 3$. When co-cultured with NCs, no significant difference was found compared to the control group in Fe content. However, when co-cultured with NPs, a significant increase in Fe content was measured for all exposure time. **Fig. S5**. Effect of Zn0.3Fe2.7O4 NCs (50 μg/mL) photothermia on H. pylori growth inhibition. Percentage of H. pylori growth inhibition (A) as a function of temperature, $t = 20$ min; (B) as a function of time, temperature = 41 °C. **Fig. S6**. Comparison of H. pylori NCTC 11637 growth inhibition between NPs and NCs heating. NCs (50 μg/mL) group showed higher growth inhibition rate (%) than NPs (50 μg/mL) group after heating induced by NIR laser to 41℃ for 20 min ($n = 3$). **Fig. S7**. Effects of NCs heating on H. pylori NCTC 11637 vacuolization and adhesion ability. Under the near-infrared (808nm) irradiation to 41℃ for 20 min, the NCs+heating group showed significant inhibition of vacuolization and adhesion ability, compared with control group (*** P<0.001). The near infrared group, NCs no heating group and water bath (41℃) group showed no difference ($n = 5$). **Fig. S8**. Changes of H. pylori NCTC 11637 antibiotic susceptibility to levofloxacin. The minimum inhibitory concentration (MIC) for levofloxacin was 1.4 μg/ml in control group (A), 0.3 μg/mL in the NPs heating group (B), and 0.8 μg/mL in the NCs heating group (C).

Acknowledgements

The authors thank Dr. Niall Joudeh, School of Medicine, Dentistry & Biomedical Sciences, Queen's University Belfast, United Kingdom, for his valuable opinions and language editing.

Author contributions

FSM carried out the ***H. pylori*** growth and antibiotics susceptibility experiments, performed biosafety testing and drafted the manuscript; HJT performed biofilm tests; YM and TYY carried out the preparation and characterization of nanoclusters. YJL conducted the photothermal procedure. XPW and YYG performed interpretation and evaluation of the results and wrote the manuscript. GSW designed and conceived of the study, participated in its coordination and revised the manuscript. GSW had primary responsibility for final content. All authors read and approved the final manuscript.

Funding
This study was supported by National Natural Science Foundation of China (Grant number. 51471186, 51771124), Chinese PLA Healthcare Project (Grant number 18BJZ22) and National Clinical Research Center for Geriatric Diseases (Grant number NCRCG-PLAGH-2019015). The funder had no role in the study design, data collection, data analysis, data interpretation, or writing of the article.

Availability of data and materials
All data generated or analyzed during this study are included in this published article and its supplementary information files.

Declarations

Ethics approval and consent to participate
Not applicable.

Consent for publication
Not applicable.

Competing interests
The authors declare that they have no competing interests.

Author details
[1]Department of Gastroenterology, The Second Medical Center & National Clinical Research Center for Geriatric Diseases, Chinese PLA General Hospital, Beijing 100853, People's Republic of China. [2]Department of Physics, Capital Normal University, Beijing, China. [3]School of Medicine, Dentistry & Biomedical Sciences, Queen's University Belfast, Belfast, UK.

Received: 16 December 2021 Accepted: 28 April 2022
Published online: 16 May 2022

References

Akhavan O, Meidanchi A, Ghaderi E, Khoei S (2014) Zinc ferrite spinel-graphene in magneto-photothermal therapy of cancer. J Mater Chem B 2:3306–3314
Albarqi HA, Wong LH, Schumann C, Sabei FY, Korzun T, Li X et al (2019) Biocompatible nanoclusters with high heating efficiency for systemically delivered magnetic hyperthermia. ACS Nano 13:6383–6395
Alumutairi L, Yu B, Filka M, Nayfach J, Kim MH (2020) Mild magnetic nanoparticle hyperthermia enhances the susceptibility of Staphylococcus aureus biofilm to antibiotics. Int J Hyperthermia 37:66–75
Bina JE, Alm RA, Uria-Nickelsen M, Thomas SR, Trust TJ, Hancock RE (2000) Helicobacter pylori uptake and efflux: basis for intrinsic susceptibility to antibiotics in vitro. Antimicrob Agents Chemother 44:248–254
Boyanova L, Hadzhiyski P, Kandilarov N, Markovska R, Mitov I (2019) Multidrug resistance in Helicobacter pylori: current state and future directions. Expert Rev Clin Pharmacol 12:909–915
Cai Y, Wang C, Chen Z, Xu Z, Li H, Li W et al (2020) Transporters HP0939, HP0497, and HP0471 participate in intrinsic multidrug resistance and biofilm formation in Helicobacter pylori by enhancing drug efflux. Helicobacter 25:e12715
Cammarota G, Sanguinetti M, Gallo A, Posteraro B (2012) Review article: biofilm formation by Helicobacter pylori as a target for eradication of resistant infection. Aliment Pharmacol Ther 36:222–230
Cheng W, Zeng X, Chen H, Li Z, Zeng W, Mei L et al (2019) Versatile polydopamine platforms: synthesis and promising applications for surface modification and advanced nanomedicine. ACS Nano 13:8537–8565
Coldham NG, Webber M, Woodward MJ, Piddock LJ (2010) A 96-well plate fluorescence assay for assessment of cellular permeability and active efflux in Salmonella enterica serovar Typhimurium and *Escherichia coli*. J Antimicrob Chemother 65:1655–1663
de Souza MPC, de Camargo BAF, Sposito L, Fortunato GC, Carvalho GC, Marena GD et al (2021) Highlighting the use of micro and nanoparticles based-drug delivery systems for the treatment of Helicobacter pylori infections. Crit Rev Microbiol 47:435–460
Debbage P, Jaschke W (2008) Molecular imaging with nanoparticles: giant roles for dwarf actors. Histochem Cell Biol 130:845–875
European-Committee. The European Committee on antimicrobial susceptibility testing. breakpoint tables for interpretation of MICs and zone diameters. Version 11.0, 2021. http://www.eucast.org.
Fanelus I, Desrosiers RR (2013) Mitochondrial uncoupler carbonyl cyanide M-chlorophenylhydrazone induces the multimer assembly and activity of repair enzyme protein L-isoaspartyl methyltransferase. J Mol Neurosci 50:411–423
Fang CH, Tsai PI, Huang SW, Sun JS, Chang JZ, Shen HH et al (2017) Magnetic hyperthermia enhance the treatment efficacy of peri-implant osteomyelitis. BMC Infect Dis 17:516
Flemming HC, Wingender J, Szewzyk U, Steinberg P, Rice SA, Kjelleberg S (2016) Biofilms: an emergent form of bacterial life. Nat Rev Microbiol 14:563–575
Forman D, Graham DY (2004) Review article: impact of Helicobacter pylori on society-role for a strategy of "search and eradicate." Aliment Pharmacol Ther 19(Suppl 1):17–21
Forte M, Iachetta G, Tussellino M, Carotenuto R, Prisco M, De Falco M et al (2016) Polystyrene nanoparticles internalization in human gastric adenocarcinoma cells. Toxicol in Vitro 31:126–136
Freedberg DE, Lebwohl B, Abrams JA (2014) The impact of proton pump inhibitors on the human gastrointestinal microbiome. Clin Lab Med 34:771–785

Gratton SE, Ropp PA, Pohlhaus PD, Luft JC, Madden VJ, Napier ME et al (2008) The effect of particle design on cellular internalization pathways. Proc Natl Acad Sci U S A 105:11613–11618
Gurunathan S, Jeong JK, Han JW, Zhang XF, Park JH, Kim JH (2015) Multidimensional effects of biologically synthesized silver nanoparticles in Helicobacter pylori, Helicobacter felis, and human lung (L132) and lung carcinoma A549 cells. Nanoscale Res Lett 10:35
Han D, Han Y, Li J, Liu X, Yeung KWK, Zheng Y et al (2020) Enhanced photocatalytic activity and photothermal effects of cu-doped metal-organic frameworks for rapid treatment of bacteria-infected wounds. Appl Catal B Environ 261:118248
Hassan HF, Mansour AM, Abo-Youssef AM, Elsadek BE, Messiha BA (2017) Zinc oxide nanoparticles as a novel anticancer approach; in vitro and in vivo evidence. Clin Exp Pharmacol Physiol 44:235–243
Hathroubi S, Servetas SL, Windham I, Merrell DS, Ottemann KM (2018) Helicobacter pylori Biofilm Formation and Its Potential Role in Pathogenesis. Microbiol Mol Biol Rev 82:e00001
He S, Zhang H, Liu Y, Sun F, Yu X, Li X et al (2018) Maximizing specific loss power for magnetic hyperthermia by hard-soft mixed ferrites. Small 14(29):e1800135
Høiby N, Bjarnsholt T, Givskov M, Molin S, Ciofu O (2010) Antibiotic resistance of bacterial biofilms. Int J Antimicrob Agents 35:322–332
Hoshyar N, Gray S, Han H, Bao G (2016) The effect of nanoparticle size on in vivo pharmacokinetics and cellular interaction. Nanomedicine (lond) 11:673–692
Huang Y, Wang QL, Cheng DD, Xu WT, Lu NH (2016) Adhesion and invasion of gastric mucosa epithelial cells by Helicobacter pylori. Front Cell Infect Microbiol 6:159
Ierardi E, Giorgio F, Losurdo G, Di Leo A, Principi M (2013) How antibiotic resistances could change Helicobacter pylori treatment: a matter of geography? World J Gastroenterol 19:8168–8180
Jaque D, Martínez Maestro L, del Rosal B, Haro-Gonzalez P, Benayas A, Plaza JL et al (2014) Nanoparticles for photothermal therapies. Nanoscale 6:9494–9530
Kim S, Lee SY, Cho HJ (2018) Berberine and zinc oxide-based nanoparticles for the chemo-photothermal therapy of lung adenocarcinoma. Biochem Biophys Res Commun 501:765–770
Kusters JG, van Vliet AH, Kuipers EJ (2006) Pathogenesis of Helicobacter pylori infection. Clin Microbiol Rev 19:449–490
Kwon DH, Dore MP, Kim JJ, Kato M, Lee M, Wu JY et al (2003) High-level beta-lactam resistance associated with acquired multidrug resistance in Helicobacter pylori. Antimicrob Agents Chemother 47:2169–2178
Li J, Liu X, Tan L, Cui Z, Yang X, Liang Y et al (2019) Zinc-doped Prussian blue enhances photothermal clearance of Staphylococcus aureus and promotes tissue repair in infected wounds. Nat Commun 10:4490
Li Z, Yang Y, Wei H, Shan X, Wang X, Ou M et al (2021) Charge-reversal biodegradable MSNs for tumor synergetic chemo/photothermal and visualized therapy. J Control Release 338:719–730
Liu ZQ, Zheng PY, Yang PC (2008) Efflux pump gene hefA of Helicobacter pylori plays an important role in multidrug resistance. World J Gastroenterol 14:5217–5222
Liu G, Zou J, Tang Q, Yang X, Zhang Y, Zhang Q et al (2017) Surface modified Ti(3)C(2) MXene nanosheets for tumor targeting photothermal/photodynamic/chemo synergistic therapy. ACS Appl Mater Interfaces 9:40077–40086
Liu L, Pan X, Liu S, Hu Y, Ma D (2021) Near-infrared light-triggered nitric oxide release combined with low-temperature photothermal therapy for synergetic antibacterial and antifungal. Smart Mater Med 2:302–313
Ma M, Liu X, Tan L, Cui Z, Yang X, Liang Y et al (2019) Enhancing the antibacterial efficacy of low-dose gentamicin with 5 minute assistance of photothermy at 50 °C. Biomater Sci 7:1437–1447
Mane SP, Dominguez-Bello MG, Blaser MJ, Sobral BW, Hontecillas R, Skoneczka J et al (2010) Host-interactive genes in Amerindian Helicobacter pylori diverge from their Old World homologs and mediate inflammatory responses. J Bacteriol 192:3078–3092
McColl KE (2010) Clinical practice. Helicobacter pylori infection. N Engl J Med 362:1597–1604
Nguyen M, Mikita G, Hoda RS (2016) "Intercellular bridges" in a case of well differentiated squamous carcinoma. Diagn Cytopathol 44:121–123
Palframan SL, Kwok T, Gabriel K (2012) Vacuolating cytotoxin A (VacA), a key toxin for Helicobacter pylori pathogenesis. Front Cell Infect Microbiol 2:92
Parkin DM (2006) The global health burden of infection-associated cancers in the year 2002. Int J Cancer 118:3030–3044
Peake RW, Marsden DL, Bodamer OA, Gelb MH, Millington DS, Wijburg F (2016) Newborn screening for lysosomal storage disorders: Quo Vadis? Clin Chem 62:1430–1438
Revia RA, Zhang M (2016) Magnetite nanoparticles for cancer diagnosis, treatment, and treatment monitoring: recent advances. Mater Today (kidlington) 19:157–168
Riedinger A, Guardia P, Curcio A, Garcia MA, Cingolani R, Manna L et al (2013) Subnanometer local temperature probing and remotely controlled drug release based on azo-functionalized iron oxide nanoparticles. Nano Lett 13:2399–2406
Rocha GA, Rocha AM, Gomes AD, Faria CL Jr, Melo FF, Batista SA et al (2015) STAT3 polymorphism and Helicobacter pylori CagA strains with higher number of EPIYA-C segments independently increase the risk of gastric cancer. BMC Cancer 15:528
Sahay G, Alakhova DY, Kabanov AV (2010) Endocytosis of nanomedicines. J Control Release 145:182–195
Şen Karaman D, Ercan UK, Bakay E, Topaloğlu N, Rosenholm JM (2020) Evolving technologies and strategies for combating antibacterial resistance in the advent of the postantibiotic era. Adv Funct Mater 30(15):1908783
Tacconelli E, Carrara E, Savoldi A, Harbarth S, Mendelson M, Monnet DL et al (2018) Discovery, research, and development of new antibiotics: the WHO priority list of antibiotic-resistant bacteria and tuberculosis. Lancet Infect Dis 18:318–327
Takenaka S, Iwaku M, Hoshino E (2001) Artificial Pseudomonas aeruginosa biofilms and confocal laser scanning microscopic analysis. J Infect Chemother 7:87–93
Teng CP, Zhou T, Ye E, Liu S, Koh LD, Low M et al (2016) Effective targeted photothermal ablation of multidrug resistant bacteria and their biofilms with NIR-absorbing gold nanocrosses. Adv Healthc Mater 5:2122–2130

Uemura N, Okamoto S, Yamamoto S, Matsumura N, Yamaguchi S, Yamakido M et al (2001) Helicobacter pylori infection and the development of gastric cancer. N Engl J Med 345:784–789
van Amsterdam K, Bart A, van der Ende A (2005) A Helicobacter pylori TolC efflux pump confers resistance to metronidazole. Antimicrob Agents Chemother 49:1477–1482
van den Berg van Saparoes HB, Lubelski J, van Merkerk R, Mazurkiewicz PS, Driessen AJ (2005) Proton motive force-dependent Hoechst 33342 transport by the ABC transporter LmrA of Lactococcus lactis. Biochemistry 44:16931–16938
Vimala K, Shanthi K, Sundarraj S, Kannan S (2017) Synergistic effect of chemo-photothermal for breast cancer therapy using folic acid (FA) modified zinc oxide nanosheet. J Colloid Interface Sci 488:92–108
Wu T, Wang L, Gong M, Lin Y, Xu Y, Ye L et al (2019) Synergistic effects of nanoparticle heating and amoxicillin on H. pylori inhibition. J Magn Magn Mater 485:95–104
Yang SJ, Huang CH, Yang JC, Wang CH, Shieh MJ (2020) Residence time-extended nanoparticles by magnetic field improve the eradication efficiency of Helicobacter pylori. ACS Appl Mater Interfaces 12:54316–54327
Yonezawa H, Osaki T, Kamiya S (2015) Biofilm formation by Helicobacter pylori and its involvement for antibiotic resistance. Biomed Res Int 2015:914791
Yu S, Li G, Zhao P, Cheng Q, He Q, Ma D et al (2019) NIR-laser-controlled hydrogen-releasing PdH nanohydride for synergistic hydrogen-photothermal antibacterial and wound-healing therapies. Adv Funct Mater 29:1905697
Yuan Z, Tao B, He Y, Mu C, Liu G, Zhang J et al (2019) Remote eradication of biofilm on titanium implant via near-infrared light triggered photothermal/photodynamic therapy strategy. Biomaterials 223:119479
Zeng X, Liu G, Tao W, Ma Y, Zhang X, He F et al (2017) A drug-self-gated mesoporous antitumor nanoplatform based on pH-sensitive dynamic covalent bond. Adv Funct Mater 27:1605985
Zhang Z, Liu ZQ, Zheng PY, Tang FA, Yang PC (2010) Influence of efflux pump inhibitors on the multidrug resistance of Helicobacter pylori. World J Gastroenterol 16:1279–1284
Zhang J, Chen Z, Kong J, Liang Y, Chen K, Chang Y et al (2020) Fullerenol nanoparticles eradicate Helicobacter pylori via pH-responsive peroxidase activity. ACS Appl Mater Interfaces. https://doi.org/10.1021/acsami.0c05509
Zhi X, Liu Y, Lin L, Yang M, Zhang L, Zhang L et al (2019) Oral pH sensitive GNS@ab nanoprobes for targeted therapy of Helicobacter pylori without disturbance gut microbiome. Nanomedicine 20:102019

Publisher's Note